HHS Public Access

Author manuscript

Magn Reson Med. Author manuscript; available in PMC 2023 February 01.

Published in final edited form as:

Magn Reson Med. 2022 February ; 87(2): 904–914. doi:10.1002/mrm.28989.

Self-supervised IVIM DWI parameter estimation with a physics based forward model

Serge Didenko Vasylechko[1,2,*], **Simon K. Warfield**[1,2], **Onur Afacan**[1,2,†], **Sila Kurugol**[1,2,†]

[1]Computational Radiology Laboratory, Boston Children's Hospital, Boston, MA, USA

[2]Harvard Medical School, Boston, MA, USA

Abstract

Purpose: To assess the robustness and repeatability of intravoxel incoherent motion model (IVIM) parameter estimation for the diffusion weighted MRI in the abdominal organs under the constraints of noisy diffusion signal using a novel neural network method.

Methods: Clinically acquired abdominal scans of Crohn's disease patients were retrospectively analyzed with regions segmented in the kidney cortex, spleen, liver and bowel. A novel IVIM parameter fitting method based on the principle of a physics guided self-supervised convolutional neural network that does not require reference parameter estimates for training was compared to a conventional non linear least squares (NNLS) algorithm, and a voxelwise trained artificial neural network (ANN).

Results: Results showed substantial increase in parameter robustness to the noise corrupted signal. In an intra-session repeatability experiment, the proposed method showed reduced coefficient of variation (CoV) over multiple acquisitions in comparison to conventional NLLS method and comparable performance to ANN. The use of D and f estimates from the proposed method led to the smallest misclassification error in linear discriminant analysis for characterization between normal and abnormal Crohn's disease bowel tissue. The fitting of $D*$ parameter remains to be challenging.

Conclusion: The proposed method yields robust estimates of D and f IVIM parameters under the constraints of noisy diffusion signal. This indicates a potential for the use of the proposed method in conjunction with accelerated DW-MRI acquisition strategies, which would typically result in lower signal to noise ratio.

Keywords

self-supervised; IVIM; abdominal; diffusion; parameter estimation; pediatric

[*]Corresponding author: Name Serge Didenko Vasylechko, Department Computational Radiology Laboratory, Institute Boston Children's Hospital, Address 360 Longwood Avenue, Boston, MA, 02215, USA, serge.vasylechko@childrens.harvard.edu.
[†]These authors contributed equally to this work.

Introduction

Diffusion weighted MRI (DW-MRI) enables an indirect estimate of the parameters that govern tissue microstructure including cell density, microperfusion, and cell membrane viability (21). The simplest model of DW-MRI model signal is given by a single exponential decay, which is driven by an apparent diffusion coefficient (ADC) of the tissue (8). This study focusses on a bi-exponential model of signal decay in the DW-MRI signal, an intravoxel incoherent motion (IVIM) model, which recognizes that diffusion in tissue occurs at two scales due to the complex varying cell structures and contribution from vascular flow in microcapillaries. IVIM encapsulates both slow and fast diffusion processes has been shown to hold an increased benefit in comparison to the ADC model for the assessment of severity of a variety of clinical conditions such as renal dysfunction, tumours, liver fibrosis and assessment of bowel inflammation and fibrosis in Crohn's disease (34; 37; 19; 16).

IVIM model is described by:

$$S(b) = S_0\left(fe^{-bD^*} + (1-f)e^{-bD}\right)$$

where b is the vector of diffusion weightings (b-values), S_0 is the non-diffusion dependent MR signal, D is the diffusion coefficient associated with slow diffusion of water molecules, $D*$ is the diffusion coefficient linked to the fast diffusion due to water molecule perfusion in microcapillaries and f is the perfusion fraction that relates to the volume fraction of microcapillaries' contributions to the diffusion.

In a 2D MR acquisition, each diffusion signal is obtained at a certain b-value and a certain diffusion-sensitizing gradient. For IVIM parameter fitting, diffusion sensitizing gradient images of the same b-value can be geometrically averaged to improve the signal to noise ratio (SNR), and to average out non-isotropic diffusion properties of the tissue. However, each additional diffusion gradient image linearly scales the acquisition time.

In clinical practice, a trade-off must be made between a higher number of required images to improve the robustness of the IVIM parameter estimates and requirement to minimize the scan time to lessen motion artifacts, patient discomfort and cost to the medical facility. This is especially important in pediatric population, which calls for a reduction in the use of sedation and anaesthesia. Scan time reduction in DW-MRI is conventionally achieved via a reduction in the number of b-values, diffusion gradients, signal averages (NSA) or via in-plane accelerated imaging. Novel acceleration methods, such as simultaneous multi-slice imaging (SMS), have also shown promise for the use in fast DW-MRI (15). The goal of this study was to investigate the robustness and repeatability of IVIM parameter fitting under the constraints of low SNR input, which is typically associated with a reduction in the number of available diffusion gradients, higher in-place acceleration factors or SMS.

The most common approaches to the estimation of quantitative MRI parameters of the IVIM model are performed on a voxel wise basis via non-linear least squares (NLLS) methods (20). These approaches suffer from poor precision and repeatability, which can be improved by integrating the estimates over spatially homogeneous priors (33). Bayesian methods have

also been used to model the whole diffusion spectrum in terms of probability distribution rather than as a two compartmental model to further reduce variability (20). However, these methods are significantly slower and typically take hours to fit for a single patient, rendering them unfeasible for real-time clinical use.

Advances in deep learning methods have shown robust performance on noise corrupted MRI signals and superior computational speed (27). Conventional deep learning architectures are typically trained in a supervised manner, which poses a drawback for IVIM model fitting due to lack of a robust conventional method for parameter estimation with high accuracy and precision that can be used as a reference in parameter estimates. The performance of supervised training cannot surpass robustness and accuracy of the reference model. In the instance of conventional IVIM methods, the variability of D* estimates is significantly high even with Bayesian methods and thus the use of such ground truth reference is not commendable (12).

To address this limitation, neural networks can be trained in an unsupervised manner on synthetically generated data. This is achieved by sampling IVIM parameter values within the acceptable bounds of D, $D*$ and f, from which the DW-MRI signal is estimated using the IVIM equation. This voxelwise synthetic dataset generation approach has been used to train feedforward artificial neural networks (ANNs) in a voxelwise manner (4; 2; 9; 6). Alternatively, the input data itself can be used to train neural networks in a self-supervised manner, without the need for reference labels (13).

However, neural networks trained in a voxelwise manner do not incorporate any prior knowledge of the spatial homogeneity in tissues of the same class, and therefore performance may suffer in the conditions of low SNR. Convolutional neural networks have been successful in capturing the spatial dependency between neighbouring voxels to effectively denoise the low SNR DW-MRI data, and conventional parameter estimation schemes could then be applied for model fitting (14; 7). However, it has also been shown that convolutional neural networks, such as the U-net architecture (32), can directly estimate parameters from noisy MRI signal in a self-supervised manner for modelling $T1$, $T2$ and $T2*$ decay constants (24; 29; 35).

In this work we evaluate a self-supervised convolutional neural network for direct estimation of IVIM parameters on noisy SNR input. The network is trained directly on clinical Crohn's patient data and does not require supervision from conventional IVIM parameter fitting methods.

Methods

Data

Acquisition—DW-MRI data was acquired with a 1.5T scanner (Magnetom Avanto, Siemens Medical Solutions) using free-breathing single-shot echo-planar imaging with parameters: repetition/echo time (TR/TE) = 7500/77ms; matrix size =192×156; field of view =300×260mm; slice thickness/gap = 5mm/0mm; 36–44 axial slices; 7 b-

values=0,50,100,200,400,600,800 s/mm2 with 6 directions and 1 excitation (NSA); partial Fourier factor 6/8 and GRAPPA factor 2; acquisition time = 5.5min.

Patient population—Training, validation and test data consisted of clinically acquired axial DW-MR images from pediatric Crohn's disease patients that were used under the approved IRB protocol. The clinical dataset consisted of 134 subjects, which covered upper and lower abdominal areas. The upper abdominal organs are expected to be normal in this patient population.

Image analysis—IVIM parameter estimates in the upper portion of the abdomen were measured over three selected regions of interest - the kidney cortex, the spleen and the liver, as shown in Figure 3. Kidney medulla were excluded from the analysis due to the anisotropic nature of diffusion in these regions. Similarly, in the segmented regions of the liver, the vessel structures were also avoided due to presence of large scale perfusion in these regions, which gives rise to anisotropic signal characteristics. Each manually segmented image was cross-checked by a second observer (see co-author, S.K.) with 7 years of expertise in the abdominal IVIM analysis.

Additionally, normal and abnormal tissue in the bowel region of Crohn's disease patients' scans was marked by a trained radiologist with 2×2 voxels markings on high b-value images (b400, b600 or b800).

Architecture of the Learning Model—The parameter fitting neural network architecture is shown in Figure 1, which consists of a convolutional neural network (CNN) that solves the inverse problem by estimating the four parameters of the IVIM model from the measured signal at multiple b-values. A loss function is formed of an IVIM forward model that takes the network predicted parameters and computes the original input image at each b-value using the IVIM signal model, and from which a L2 norm of the difference between the images at the output of the forward model and the original input data to the network is optimized. No ground truth parameters are needed for training the network.

The network uses a conventional U-net (32) as a choice of CNN architecture, which is motivated by U-net's excellent performance on a number of medical imaging tasks, including self-supervised forward model based parameter regression in other domains (35; 30; 24). The U-net takes as an input sets of 3D input arrays. Each 3D array is composed of a 2D slice with a 7 dimensional vector of the DW-MRI magnitude signals of different b-values. The 3D input array is down-sized into 1024 kernels of shape 10×12 in the bottleneck layer of the U-net, and reformed back into the 3D shape that consists of the equivalent 2D slice size and a 4 dimensional vector that represents the estimated IVIM parameters at the output.

Each downsampling block of the U-net, and its equivalent upsampling block, consist of a chain of 3 sets of operations - 3×3 convolution, Relu activation and dropout. There are 4 downsampling and upsampling blocks in the U-net. The first and last convolutional operations are of the same shape as the 2D slice in the x-y dimensions and have 64 filters in the z dimension. As is common in the conventional U-net designs, the filter number is

progressively increased by a factor of 2 while the x-y dimensions are decreased by the same amount through each downsampling block, thereby leading to a 10×12×1024 array in the bottleneck layer.

Training—The dataset was split into 120 training subjects, 4 validation subjects and 10 test subjects. Validation loss was used to monitor network performance and to prevent overfitting. The following final hyper-parameters were used for training: a dropout rate of 10%, batch size of 2, 80 epochs and an Adam optimizer with a progressively decreasing learning rate over the training epochs. The framework was trained on Nvidia Titan XP GPU using Tensorflow 1.13 library (1).

Thresholding, normalization and rescaling—Prior to training, the input data was preprocessed to ensure smooth gradient flow in the backward pass of the CNN and the speed of convergence. First, the signal outside of abdominal cavity was set to zero in each image. Next, each vector of 7 b-values for each pixel in the 3D input array was normalized with respect to the mean of the first b-value image. At test time, the IVIM parameters estimated by the U-net had to be re-scaled to match the expected quantitative range of the underlying MRI signal properties.

Evaluation

Competing Methods—The proposed approach was compared to a voxelwise IVIM fitting algorithm that uses a NLLS iterative scheme via the BOBYQA method (31). BOBYQA method has been shown to improve estimates over the conventional Levenberg-Marquardt algorithms (18; 17). NNLS scheme incorporated a segmented fit approach (26) with the estimates bounded to the naturally occuring range of values for D, $D*$ and f. Additionally, we trained an ANN on synthetically generated dataset, similar to (4; 2). Synthetic training dataset consisted of 1,000,000 voxels and D, $D*$ and f parameters sampled from a naturally occurring range of their values. ANN consisted of 7 nodes at input (equivalent to the number of b-values), followed by three fully connected hidden layers with 7 nodes each, and 3 nodes at the output (equivalent to D, $D*$ and f). Input signal was normalized with respect to the first b-value at test time. Technical implementation was based on modifications to the code supplied by (2).

Accuracy of parameter estimates on noisy DW-MRI—Noise was added to the input DW-MRI data to evaluate each method's competence at varying levels of SNR, as shown in Figure S1. The noise was drawn from a normal distribution that was scaled with respect to the mean estimate of the signal of the abdominal cavity to ensure that the noise is scaled in relation to each scan's varying average signal intensity and hence it is drawn from a normal distribution that is scaled between $N(0, \frac{B0}{SNR})$. Performance of each method was evaluated by computing normalized root mean squared error (nRMSE) between each IVIM parameter estimate from the original input data and the parameter estimate from the noise corrupted input data. nRMSE was computed in a pairwise manner on a voxel by voxel basis for all slices of all subjects for each parameter and segmented region. Normalization was performed by dividing RMSE by the mean value of the given parameter estimate in

the original non noisy data for the given region, and therefore represents the percentage difference in relation to the original signal.

Repeatability—In order to assess repeatability, a separately acquired dataset of from 5 healthy volunteers with repeat intrasession acquisitions was considered. The acquisition parameters for this data were identical to those of the clinical protocol used for the training and test data. The DW-MRI acquisition was repeated multiple times within a single scan session for each of the 5 volunteers at 6,4,4,3,3 repetitions respectively. A carefully placed small region of interest that consisted of 12 voxels was placed in three preset regions of interest. Coefficient of variation (CoV) between repetitions was estimated for each patient for each parameter for each region for each subject.

Crohn's disease tissue characterization—In this experiment we evaluated the ability of each parameter estimation method to discriminate between tissue class types in a clinically relevant region of interest. Linear discriminant analysis (LDA) aims to find the best decision boundary to separate class variables with a linear combination of dependent variables. LDA was performed on the estimated IVIM parameters as dependent variables. Misclassification error rate of the estimated LDA linear discriminator function was evaluated for D, $D*$, f and their joint combinations. In each test, a diagonal covariance matrix estimate between dependent variables was used to fit a multivariate normal density to each class. Training data consisted of all voxels for all patients in the Crohn's diseased scans that were marked by the trained radiologist, which made up 160 voxels per class. LDA was performed with the Matlab software(25).

Results

Estimated parameter maps from an example slice are shown in Figure 2 with kidneys, spleen and liver clearly visible in axial view. A difference image is also shown between the proposed method and each of the two competing methods. Qualitative assessment of the proposed method shows excellent agreement with NNLS and voxelwise trained artificial neural network (ANN) for the estimation of D parameter, which is the parameter that is typically more robust and easier to fit (23). The proposed method shows a less noisy estimate of the D* parameter such that it is possible to view the outlines of the anatomy in the three preset regions of interest. Similarly, the estimate of the f parameter is well defined around the kidney structures in the proposed method.

Boxplots of the parameter estimates for each of the three preset regions of interest in the upper abdominal area are shown in Figure 5. Statistical analysis was performed to indicate significant difference in the parameter estimates between NLLS and each of the alternative fitting methods. The analysis was done with a paired Mann–Whitney–Wilcoxon non-parametric test of the null hypothesis, with adjustment for multiple comparison using the Scipy statistical toolbox (36). Statistical significance is marked with an asterisk, with ** and * indicating significance at 99% and 95% confidence interval respectively, and *ns* indicating no significant difference. Detailed breakdown of p-value stastistics are shown in Supporting Information Table 2.

Results indicated no significant difference for D between NLLS and each of the alternative fitting methods in each of the three regions of interest. Both the proposed method and ANN showed substantially lower variance in $D*$ estimates, which is typically a difficult parameter to estimate with the conventional fitting methods. No significant difference was found with NLLS for $D*$ in kidneys and liver, however significant difference was found between the estimates in spleen for both ANN and the proposed methods. Similarly, lower variability was observed in the estimates of f parameter in spleen for ANN and the proposed method. The scale of variability in D was an order of magnitude lower than in $D*$, and two orders of magnitude lower in D, which is consistent with relative stability of the f parameter. Significant difference was found in parameter estimates of f for ANN and the proposed method in the kidney region of interest.

Accuracy of parameter estimates on noisy DW-MRI

Results in Figure 6 show significant reduction in nRMSE for all regions of interest in D and $D*$ with the proposed method. Reduction is more pronounced when comparing the proposed method with the NNLS method. However, note that nRMSE in $D*$ varies on a substantially larger scale when compared to D, particularly for NNLS. Finally, some improvement in nRMSE is shown for the estimation in f with the proposed method, although it is less pronounced.

Repeatability

Mean CoV measure across 5 subjects for each region and for each parameter are shown in Figure 7. Results indicate reduction in CoV for $D*$ for both neural network approaches, when compared to NLLS. A smaller reduction is seen in liver and spleen between NLLS and the two neural network methods for D, and similarly for kidneys and spleen for f parameter. Interestingly, both neural network approaches show higher CoV in the liver for f parameter. In general, the proposed method shows reduced CoV over the voxelwise trained neural network. However, it is also noted that the proposed method has a higher CoV in kidneys and spleen for D, and kidneys and liver for f.

Crohn’s disease tissue characterization

Results of LDA based linear classifier between normal and abnormal Crohn’s disease tissue that was estimated with D and f parameters is shown in Figure 8. Misclassification error rate (err) in class estimates from the available data is shown at the top of each graph. The proposed approach yields the lower misclassification error for the fitted linear discriminant functions as more data points in the D vs f plot are clustered together. Visual evaluation between normal and abnormal appearing tissue of the method is given in Figure 4, and statistical aggregate across all subjects are shown in Figure 9. Supporting Information Table 1 provides misclassification error rate for each method when different combinations of IVIM parameters are used to build the linear discriminant function. Notably, neither of the methods could provide reliable linear discriminant function with the use of $D*$ parameter. The use of both D and f parameters jointly had improved the classification performance for both neural network methods, in contrast to when each parameter is used independently.

Discussion

This study evaluated a self-supervised convolution neural network based method for estimation of IVIM parameters from multi b-value diffusion weighted images on clinically acquired DW-MRI data of Crohn's disease patients. The proposed method was compared to the conventional iterative voxelwise NLLS fitting scheme as well as a voxelwise synthetically trained artificial neural network. Analysis of the regions of interest consisted of spleen, kidney cortex, liver and bowel regions. Results indicate improved robustness of IVIM parameter estimates in the presence of noise, as well as reduced variability in the intra-session repeatability experiments. The proposed method was able to provide reliable estimates of D and f parameters that can be used to distinctly characterize between abnormal and normal tissue in the bowel regions of Crohn's disease patients via linear discriminant analysis.

The proposed neural network architecture consisted of the widely successful U-net (32), which regresses parameter estimates for each voxel from a set of spatially dependent convolutional operations in a self supervised manner. It has been shown previously that learned priors that incorporate the knowledge of the spatial consistency and the knowledge of the underlying data distribution can effectively denoise the input while regressing estimates to a true value (3). This may indicate the improved performance of the proposed algorithm in the presence of noise over the voxel-based fitting methods in the present study.

The robustness of the proposed method to low SNR input indicates a potential for IVIM parameter estimation with certain accelerated acquisition strategies that typically lead to low SNR images, such as acquisitions with a reduced number of diffusion gradients, higher in-plane acceleration factors or simultaneous multi-slice imaging. Our results showed that nRMSE error of less than 0.15 for f and less than 0.1 for D is achievable with relative SNR decreased to 50, which indicates that acceleration factors of up to 4x may potentially be investigated in the future studies. Additional data collected on a cohort of healthy volunteers with these accelerated strategies is required to be evaluated first in conjunction with the proposed fitting method. Importantly, motion between images acquired at different b-values and at directional gradients remains to be an active issue that needs to be addressed. In future work, application of motion correction methods such as in the work of Kurugol et al. (17) would be of benefit.

It is important to note that the present study's clinically approved acquisition protocol had already included a number of accelerated scanning strategies and therefore, this limited some investigation into how these factors may affect performance of the proposed fitting approach. Namely, the data was acquired with the minimum number of signal averages (NSA=1), a high partial Fourier factor (0.625), a GRAPPA factor of 2 and only 7 b-values.

While $D*$ estimates obtained with the proposed method showed reduced variability, the use of this parameter remains to be impractical due to degeneracy in $D*$ values. This is supported by the evaluation of $D*$ in the linear discriminant analysis experiment for the characterization of abnormal Crohn's disease tissue in the bowel. Prior literature suggests

that robust fit of this parameter requires a significantly higher number of b-values (11), which would be impractical within the constraints of clinically feasible acquisition times.

Further improvements to parameter fitting accuracy for the proposed method may include constraints on the bounds of each parameter, similarly to those applied in the BOBYQA based NNLS fitting algorithm. This has recently been demonstrated within the context of a neural network where the output of the final layer of the voxelwise trained network was multiplied with a sigmoid function, and then normalized within the minimum-maximum range of each parameter (13).

The added benefit of neural networks is their superior computational speed during inference. Notably, the ANN took on average 3 seconds per subject for IVIM parameter estimation, the proposed method 5 seconds and NNLS method 28 seconds. Slightly longer inference time for the proposed method over the ANN is likely to be due to a larger 2D architecture that performs inference over an entire slice, rather than a single voxel. We also note that ANN was implemented in Pytorch framework (28), while the proposed network was build with Tensorflow framework (1).

Practical application of the proposed approach is affected by the common setbacks of deep learning methods, which include the need to retrain the network for inputs that are drawn from dissimilar probability distribution to that of the training set. Examples of this may be images obtained with different acquisition parameters, images of a different anatomy or a different patient class, where IVIM parameter statistics may be sufficiently distinct. To avoid retraining from scratch, transfer learning may be used in certain cases where sufficient new training data is available and the data does not differ substantially (5; 38). However, if the input shape, or the range of b-values, are different then a completely new training process is required. Moreover, it has been recently suggested that optimal b-value combinations may change based on noise statistics when training a voxelwise neural network (22). Furthermore, the work of Gyori et al. (10) suggests that uniform sampling of all possible parameter values during training generally leads to lower precision for typical parameters but more accuracy for atypical parameter estimates. A consideration for this phenomena may be important when designing a neural network with a specific clinical application in mind.

In conclusion, this work introduced a self-supervised physics model guided deep learning method to estimate the IVIM parameters from multi b-value diffusion weighted images. The method was evaluated in spleen, kidney cortex, liver and bowel regions of pediatric Crohn’s disease patients. The proposed method achieves comparable performance to conventional methods with fully sampled signal, but generates more robust estimates of parameters in the presence of noise. This result suggests that the proposed method holds promise to more robust parameter estimates for accelerated scanning where the SNR of the signal is significantly degraded.

Supplementary Material

Refer to Web version on PubMed Central for supplementary material.

Acknowledgments

This work was supported partially by the Boston Children's Hospital Translational Research Program Pilot Grant 2018, Society of Pediatric Radiology Multi-center Research Grant 2019, Crohn's and Colitis Foundation of America's (CCFA) Career Development Award and by the National Institutes of Health under award numbers R01EB019483, R21DK123569, R21EB029627, and by the grant No 2019056 from the United States-Israel Binational Science Foundation (BSF), and a pilot grant from National Multiple Sclerosis Society under Award Number PP-1905-34002.

References

1. Abadi M, Agarwal A, Barham P, Brevdo E, Chen Z, Citro C, Corrado GS, Davis A, Dean J, Devin M, Ghemawat S, Goodfellow I, Harp A, Irving G, Isard M, Jia Y, Jozefowicz R, Kaiser L, Kudlur M, Levenberg J, Mané D, Monga R, Moore S, Murray D, Olah C, Schuster M, Shlens J, Steiner B, Sutskever I, Talwar K, Tucker P, Vanhoucke V, Vasudevan V, Viégas F, Vinyals O, Warden P, Wattenberg M, Wicke M, Yu Y, Zheng X. 2015. TensorFlow: Large-scale machine learning on heterogeneous systems. Software available from tensorflow.org.
2. Barbieri S, Gurney-Champion OJ, Klaassen R, Thoeny HC. 2020. Deep learning how to fit an intravoxel incoherent motion model to diffusion-weighted mri. Magnetic resonance in medicine 83:312–321. [PubMed: 31389081]
3. Batson J, Royer L. 2019. Noise2self: Blind denoising by self-supervision. arXiv preprint arXiv:1901.11365.
4. Bertleff M, Domsch S, Weingärtner S, Zapp J, O'Brien K, Barth M, Schad LR. 2017. Diffusion parameter mapping with the combined intravoxel incoherent motion and kurtosis model using artificial neural networks at 3 t. NMR in Biomedicine 30:e3833.
5. Boit J 2020. The effectiveness of transfer learning systems on medical images. [[Doctoral thesis]]: Dakota State University. Https://scholar.dsu.edu/theses/344.
6. de Almeida Martins JP, Nilsson M, Lampinen B, Palombo M, While PT, Westin CF, Szczepankiewicz F. 2021. Neural networks for parameter estimation in microstructural mri: a study with a high-dimensional diffusion-relaxation model of white matter microstructure. bioRxiv.
7. Fadnavis S, Batson J, Garyfallidis E. 2020. Patch2self: Denoising diffusion mri with self-supervised learning. arXiv preprint arXiv:2011.01355.
8. Freiman M, Voss SD, Mulkern RV, Perez-Rossello JM, Callahan MJ, Warfield SK. 2012. In vivo assessment of optimal b-value range for perfusion-insensitive apparent diffusion coefficient imaging. Medical physics 39:4832–4839. [PubMed: 22894409]
9. Grussu F, Battiston M, Palombo M, Schneider T, Wheeler-Kingshott CAG, Alexander DC. 2020. Deep learning model fitting for diffusion-relaxometry: a comparative study. bioRxiv.
10. Gyori NG, Palombo M, Clark CA, Zhang H, Alexander DC. 2021. Training data distribution significantly impacts the estimation of tissue microstructure with machine learning. bioRxiv.
11. Iima M, Kataoka M, Kanao S, Kawai M, Onishi N, Koyasu S, Murata K, Ohashi A, Sakaguchi R, Togashi K. 2018. Variability of non-gaussian diffusion mri and intravoxel incoherent motion (ivim) measurements in the breast. Plos one 13:e0193444. [PubMed: 29494639]
12. Jalnefjord O, Andersson M, Montelius M, Starck G, Elf AK, Johanson V, Svensson J, Ljungberg M. 2018. Comparison of methods for estimation of the intravoxel incoherent motion (ivim) diffusion coefficient (d) and perfusion fraction (f). Magnetic Resonance Materials in Physics, Biology and Medicine 31:715–723.
13. Kaandorp M, Barbieri S, Klaassen R, van Laarhoven HW, Crezee H, While PT, Nederveen AJ, Gurney-Champion OJ. 2020. Improved unsupervised physics-informed deep learning for intravoxel-incoherent motion modeling and evaluation in pancreatic cancer patients. arXiv preprint arXiv:2011.01689.
14. Kawamura M, Tamada D, Funayama S, Kromrey ML, Ichikawa S, Onishi H, Motosugi U. 2021. Accelerated acquisition of high-resolution diffusion-weighted imaging of the brain with a multi-shot echo-planar sequence: Deep-learning-based denoising. Magnetic Resonance in Medical Sciences 20:99. [PubMed: 32147643]

15. Kenkel D, Barth BK, Piccirelli M, Filli L, Finkenstädt T, Reiner CS, Boss A. 2017. Simultaneous multislice diffusion-weighted imaging of the kidney: a systematic analysis of image quality. Investigative radiology 52:163–169. [PubMed: 27662577]
16. Koh DM, Collins DJ. 2007. Diffusion-weighted MRI in the body: applications and challenges in oncology. American Journal of Roentgenology 188:1622–1635. [PubMed: 17515386]
17. Kurugol S, Freiman M, Afacan O, Domachevsky L, Perez-Rossello JM, Callahan MJ, Warfield SK. 2017. Motion-robust parameter estimation in abdominal diffusion-weighted mri by simultaneous image registration and model estimation. Medical image analysis 39:124–132. [PubMed: 28494271]
18. Kurugol S, Freiman M, Afacan O, Perez-Rossello J, Callahan M, Warfield S. 2016. Spatially-constrained probability distribution model of incoherent motion (spim) for abdominal diffusion-weighted mri. Medical Image Analysis 32. doi:10.1016/j.media.2016.03.009.
19. Kurugol S, Freiman M, Afacan O, Perez-Rossello JM, Callahan MJ, Warfield SK. 2014. Spatially-constrained probability distribution model of incoherent motion (SPIM) in diffusion weighted MRI signals of crohn's disease. In: International MICCAI Workshop on Computational and Clinical Challenges in Abdominal Imaging. Springer. p. 117–127.
20. Lanzarone E, Mastropietro A, Scalco E, Vidiri A, Rizzo G. 2020. A novel bayesian approach with conditional autoregressive specification for intravoxel incoherent motion diffusion-weighted mri. NMR in Biomedicine 33:e4201. [PubMed: 31884712]
21. Le Bihan D, Breton E, Lallemand D, Aubin M, Vignaud J, Laval-Jeantet M. 1988. Separation of diffusion and perfusion in intravoxel incoherent motion MR imaging. Radiology 168:497–505. [PubMed: 3393671]
22. Lee W, Kim B, Park H. 2021. Quantification of intravoxel incoherent motion with optimized b-values using deep neural network. Magnetic Resonance in Medicine 86:230–244. [PubMed: 33594783]
23. Lemke A, Stieltjes B, Schad LR, Laun FB. 2011. Toward an optimal distribution of b values for intravoxel incoherent motion imaging. Magnetic resonance imaging 29:766–776. [PubMed: 21549538]
24. Liu F, El Fakhri G, Torriani M, Kijowski R, Tanaka M. 2021. Achieving rapid and accurate relaxometry of whole knee joint using self-supervised deep learning. In: Proceedings of the International Society for Magnetic Resonance in Medicine annual meeting (ISMRM'21). International Society for Magnetic Resonance in Medicine (ISMRM).
25. MATLAB. 2019. version 9.7 (R2019b). Natick, Massachusetts: The MathWorks Inc.
26. Merisaari H, Movahedi P, Perez IM, Toivonen J, Pesola M, Taimen P, Boström PJ, Pahikkala T, Kiviniemi A, Aronen HJ, et al. 2017. Fitting methods for intravoxel incoherent motion imaging of prostate cancer on region of interest level: Repeatability and gleason score prediction. Magnetic resonance in medicine 77:1249–1264. [PubMed: 26924552]
27. Ongie G, Jalal A, Baraniuk CAMRG, Dimakis AG, Willett R. 2020. Deep learning techniques for inverse problems in imaging. IEEE Journal on Selected Areas in Information Theory.
28. Paszke A, Gross S, Massa F, Lerer A, Bradbury J, Chanan G, Killeen T, Lin Z, Gimelshein N, Antiga L, Desmaison A, Kopf A, Yang E, DeVito Z, Raison M, Tejani A, Chilamkurthy S, Steiner B, Fang L, Bai J, Chintala S. 2019. Pytorch: An imperative style, high-performance deep learning library. In: Wallach H, Larochelle H, Beygelzimer A, d'Alché-Buc F, Fox E, Garnett R, editors. Advances in Neural Information Processing Systems 32. Curran Associates, Inc.. p. 8024–8035.
29. Pirk CM, Gómez PA, Lipp I, Buonincontri G, Molina-Romero M, Sekuboyina A, Waldmannstetter D, Dannenberg J, Endt S, Merola A, et al. 2020. Deep learning-based parameter mapping for joint relaxation and diffusion tensor mr fingerprinting. In: Medical Imaging with Deep Learning. PMLR. p. 638–654.
30. Pirkl CM, Gómez PA, Lipp I, Buonincontri G, Molina-Romero M, Sekuboyina A, Waldmannstetter D, Dannenberg J, Endt S, Merola A, et al. 2020. Deep learning-based parameter mapping for joint relaxation and diffusion tensor mr fingerprinting. arXiv preprint arXiv:2005.02020.
31. Powell MJ. 2009. The BOBYQA algorithm for bound constrained optimization without derivatives. Cambridge NA Report NA2009/06, University of Cambridge, Cambridge :26–46.

32. Ronneberger O, Fischer P, Brox T. 2015. U-net: Convolutional networks for biomedical image segmentation. In: International Conference on Medical image computing and computer-assisted intervention. Springer. p. 234–241.

33. Taimouri V, Afacan O, Perez-Rossello JM, Callahan MJ, Mulkern RV, Warfield SK, Freiman M. 2015. Spatially constrained incoherent motion method improves diffusion-weighted mri signal decay analysis in the liver and spleen. Medical physics 42:1895–1903. [PubMed: 25832079]

34. Tielbeek JA, Ziech ML, Li Z, Lavini C, Bipat S, Bemelman WA, Roelofs JJ, Ponsioen CY, Vos FM, Stoker J. 2014. Evaluation of conventional, dynamic contrast enhanced and diffusion weighted MRI for quantitative crohn's disease assessment with histopathology of surgical specimens. European radiology 24:619–629. [PubMed: 24037299]

35. Torop M, Kothapalli SV, Sun Y, Liu J, Kahali S, Yablonskiy DA, Kamilov US. 2020. Deep learning using a biophysical model for robust and accelerated reconstruction of quantitative, artifact-free and denoised images. Magnetic resonance in medicine 84:2932–2942. [PubMed: 32767489]

36. Virtanen P, Gommers R, Oliphant TE, Haberland M, Reddy T, Cournapeau D, Burovski E, Peterson P, Weckesser W, Bright J, van der Walt SJ, Brett M, Wilson J, Millman KJ, Mayorov N, Nelson ARJ, Jones E, Kern R, Larson E, Carey CJ, Polat İ, Feng Y, Moore EW, VanderPlas J, Laxalde D, Perktold J, Cimrman R, Henriksen I, Quintero EA, Harris CR, Archibald AM, Ribeiro AH, Pedregosa F, van Mulbregt P, SciPy 10 Contributors. 2020. SciPy 1.0: Fundamental Algorithms for Scientific Computing in Python. Nature Methods 17:261–272. doi:10.1038/s41592-019-0686-2. [PubMed: 32015543]

37. Zhao J, Wang Z, Liu M, Zhu J, Zhang X, Zhang T, Li S, Li Y. 2014. Assessment of renal fibrosis in chronic kidney disease using diffusion-weighted MRI. Clinical radiology 69:1117–1122. [PubMed: 25062924]

38. Zhuang F, Qi Z, Duan K, Xi D, Zhu Y, Zhu H, Xiong H, He Q. 2020. A comprehensive survey on transfer learning. Proceedings of the IEEE 109:43–76.

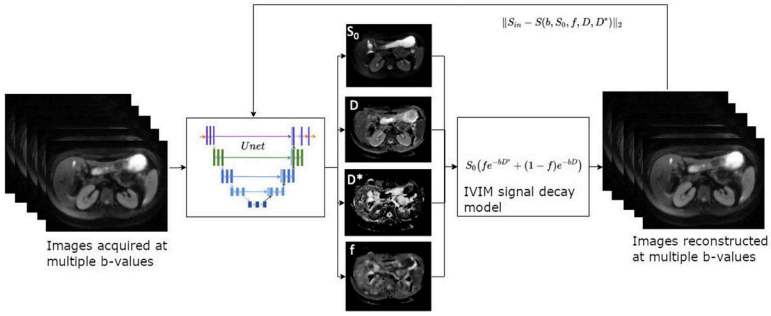

Figure 1:

A network structure of the proposed method for a physics guided IVIM parameter estimation with a self supervised U-net architecture. An input consists of 3 dimensional array, which is a concatenation of a 2D slice acquired at 7 b-values. The input is passed through a U-net to produce 4 IVIM parameter estimates at each pixel. Parameter estimates are used in the IVIM equation to reconstruct the original input image array. L2 loss between the output and the original input is used to propagate gradients backwards through the network.

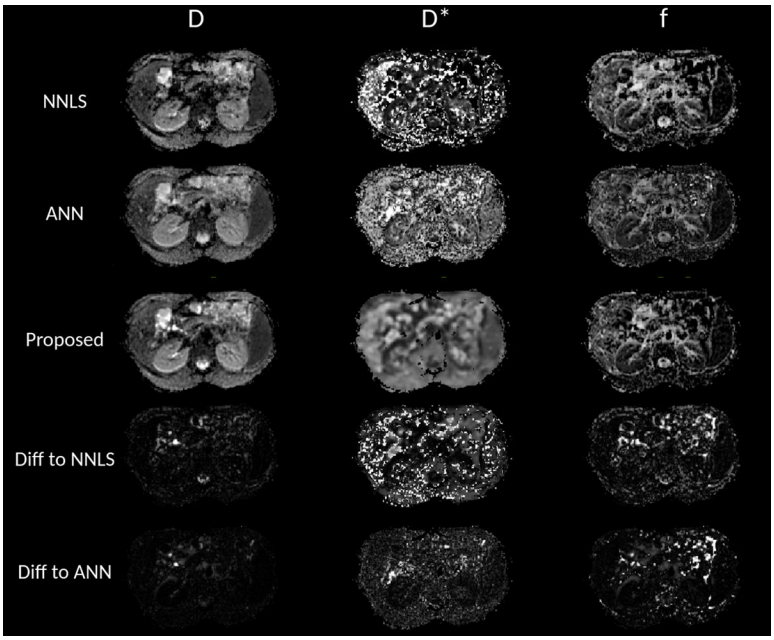

Figure 2:
An example of IVIM parameter estimates with the conventional voxelwise IVIM fitting method, ANN and the proposed approach. Difference image between the proposed method and each of the alternative methods is shown in the bottom two rows. The proposed method shows strong agreement with estimates of the conventional fitting method for the estimates of D and f, but a more coherent visual graph of D*.

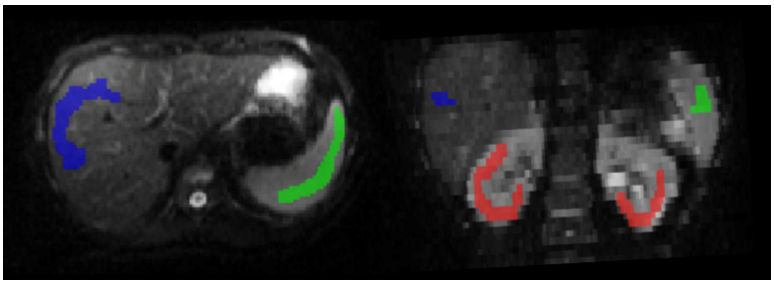

Figure 3:
An example slice of a manual segmentation of three regions of interest used for results reporting. An axial slice is shown to visualize segmentation in one of the slices over the spleen and liver. An coronal slice is included to show the segmentation over the kidney cortex area, which exhibits isotropic diffusion properties that allows for geometric averaging of input across multiple directional gradient images at each b-value.

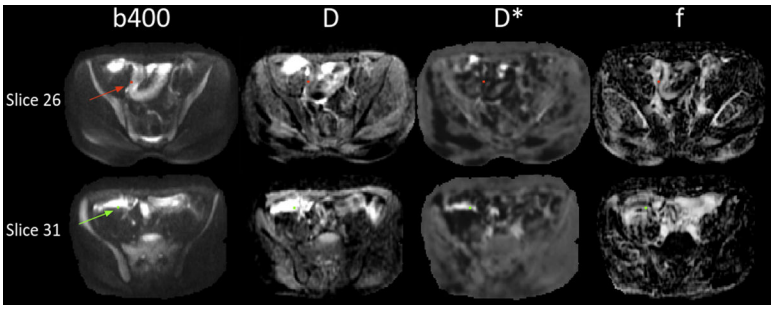

Figure 4:

Visual evaluation of Crohn's disease tissue in the bowel on b=400 b-value image and the corresponding estimated parameter maps with the proposed method. 2×2 voxel markings were labelled by a trained radiologist on high b-value images of the input data. Red labels refer to abnormal tissue and green labels refer to normal tissue.

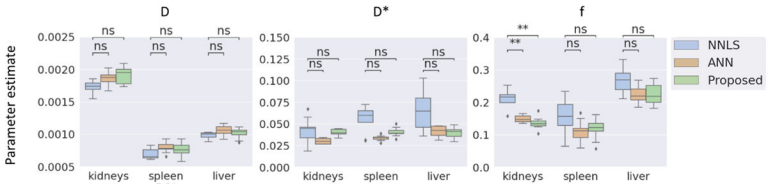

Figure 5:

IVIM parameter estimates for slow diffusion rate (*D*), fast diffusion rate (*D*∗) and perfusion fraction coefficient (*f*) for three regions of interest. A mean measure over a given region of interest for a specific parameter was measured for each subject, such that the boxplots represent the distribution over the test subjects. The legend denotes the model used to fit the data. Results of statistical analysis from the paired Mann–Whitney–Wilcoxon tests between NLLS and each of the neural network models are shown above each plot, where ∗ and ∗∗ indicate significance at 95% and 99% confidence intervals respectively.

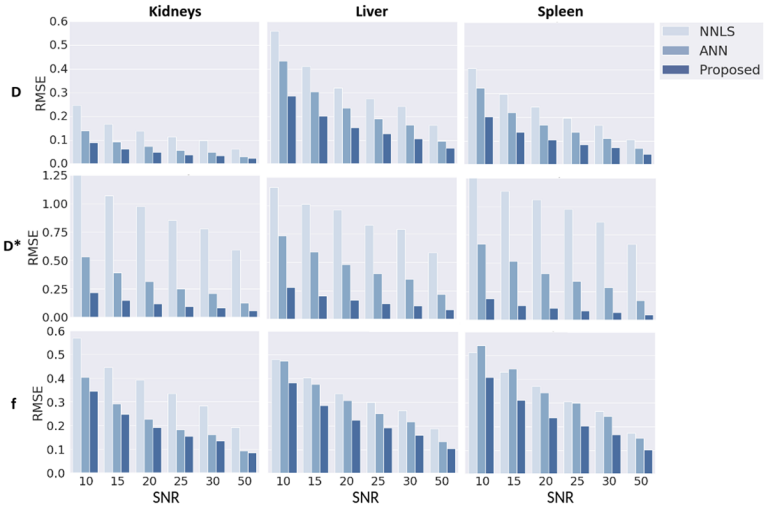

Figure 6:

Normalized root mean squared error between IVIM parameter estimates calculated on the original input data that consisted of 6 geometrically averaged diffusion gradient images at each b-value, and the noise corrupted variant of the same input at a given SNR. The proposed method shows substantial improvement in performance under the noisy input data in comparison to competing methods.

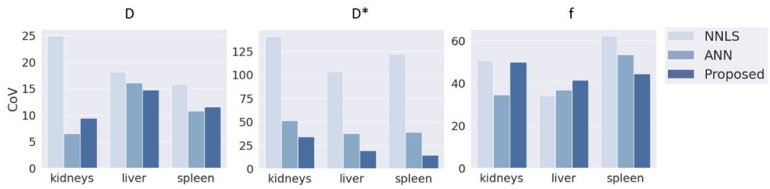

Figure 7:

Intrasession repeatability of IVIM parameter estimates computed as a coefficient of variation on a cohort of 5 healthy subjects. Both neural network methods substantially reduce CoV in $D*$ estimates in comparison to NLLS. The proposed method performs at a similar level or lower when compared to the voxelwise trained neural network.

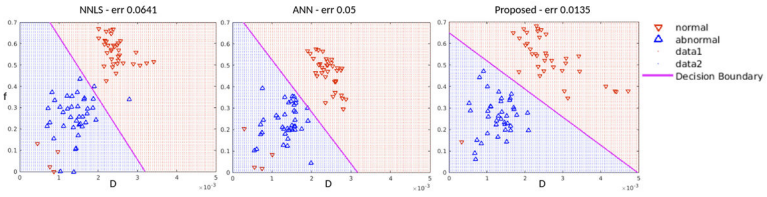

Figure 8:

Linear discriminant analysis for classification of abnormal Crohn's disease tissue in the bowel with D and f parameter estimates for each model. Misclassification error rate is based on the estimated linear discriminant function for each method by using D and f parameter estimates and is given in the subplot titles (see 'err'). All methods are able to successfully distinguish between tissue types with the proposed method yielding the lowest misclassification error rate.

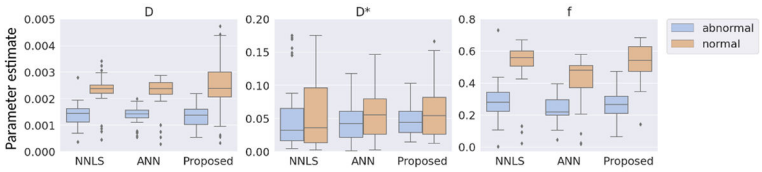

Figure 9:

IVIM parameter estimates for slow diffusion rate (*D*), fast diffusion rate (*D*∗) and perfusion fraction coefficient (*f*) in diseased and healthy regions of the bowel for Crohn's patient cohort. All methods are able to distinguish the tissue classes for *D* and *f*, however, the measure of *D*∗ yields degenerate values between the diseased and healthy tissues.